Transportation Geotechnics 46 (2024) 101246

Contents lists available at ScienceDirect

Transportation Geotechnics

journal homepage: www.elsevier.com/locate/trgeo

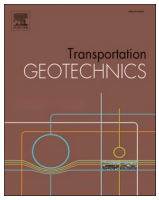

Original Article

Critical speed of ballasted railway tracks: Influence of ballast and subgrade degradation

Rakesh Sai Malisetty [a], Buddhima Indraratna [b,*]

[a] Transport Research Centre, University of Technology Sydney, Ultimo, NSW 2007, Australia
[b] Civil Engineering and Transport Research Centre, University of Technology Sydney, Ultimo, NSW 2007, Australia

ARTICLE INFO

Keywords:
Critical Speed
Dynamic Stresses
Degradation
Mud Pumping

ABSTRACT

Track substructure layers such as ballast and subgrade involve progressive degradation with time in relation to the loading history. Degradation of track components directly influences the dynamic track response including the displacements and stresses. Determining the influence of real-world substructure degradation problems such as particle breakage, ballast fouling and mud pumping on the critical speed of a given track is essential to design ballasted tracks for high-speed passenger and freight trains. In this paper, a coupled rheological-continuum model is developed to predict the track dynamic response for different train speeds and axle loads. In this novel approach, field dispersion curves obtained from MASW (Multichannel Analysis of Surface Waves) testing can be adopted along with the proposed analytical model to predict the critical speed of track as well as the corresponding dynamic stress state in the substructure layers. Analytical modelling shows that problems such as ballast fouling and mud pumping lead to reduction in the computed critical speed, while also amplifying the dynamic stress response at lower train speeds. The influence of substructure degradation is found to be more prominent for heavy-haul (freight) trains imparting higher axle loads, when compared to passenger trains. Practical insights highlighting the influence of track improvements such as placing a thicker ballast layer and the addition of a capping layer on the critical speed are presented in this study with the objective of rejuvenating future track design.

Introduction

High-speed railway networks are becoming increasingly common in many countries, and there is an increasing challenge for track engineers to build a safer and efficient railway network. In Australia, while most high-speed networks are also used by passenger trains thus demanding additional safety assurances, supply chain proponents including mining companies have proposed the need for increased operating speeds of freight trains to optimise productivity, while carrying heavier loads than ever before. The biggest challenge that arises with increasing train speeds is the amplification of track dynamic response including the transient rail displacements and associated stresses in the substructure layers. Such problems with dynamic amplification were first encountered in Ledsgard, Sweden, when X2000 train was operated at high speeds on a weak subgrade consisting of organic and peat characterised with low shear wave velocities[24,28]. Through detailed numerical investigations, it was observed that the proximity of operating train speeds to the critical speed of the track was the driving factor that had amplified the response due to resonance. The critical speed of the track is generally defined as the characteristic speed of Rayleigh waves propagated on the track surface, and their interaction with the frequency of waves generated by the moving wheel loads.

Earlier classical studies considering moving loads on a beam resting on an elastic homogenous half-space analysed the effect of train speed on dynamic behaviour of track[14]. Subsequently, several semi-analytical models were developed where the track could be modelled as a rheological system, while the wave propagation in homogenous half-space was modelled using Green's functions[27,26]. The critical speed is estimated by comparing the vertical rail displacements at different train speeds as shown in Fig. 1a. However, the ground and track substructure conditions in any railway track is layered and rarely homogenous, while determining the critical speed is often complex for a multi-layered track substructure, because the R-waves travel at different frequencies in dissimilar layers. Sheng et al. [34] proposed a semi-

* Corresponding author at: School of Civil and Environmental Engineering, Faculty of Engineering and Information Technology, University of Technology Sydney, Ultimo, NSW, Australia.
E-mail addresses: rakeshsai.malisetty@uts.edu.au (R.S. Malisetty), Buddhima.indraratna@uts.edu.au (B. Indraratna).

https://doi.org/10.1016/j.trgeo.2024.101246
Received 8 December 2023; Received in revised form 3 March 2024; Accepted 1 April 2024
Available online 2 April 2024

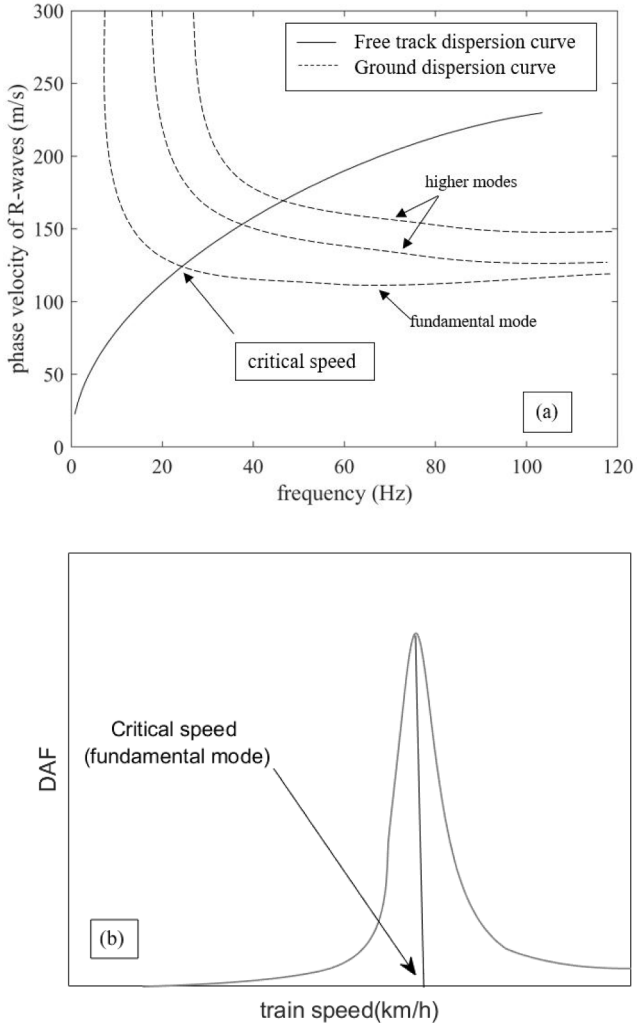

Fig. 1. (a)Direct and (b)indirect approaches for estimating critical speed of ballasted railway track.

analytical model to analyse the dynamic response of layered half-space subjected to both single oscillating load and moving loads. The interactions between different material layers of the natural ground (subgrade) and track were investigated using dispersion curves. A similar approach for interpreting dispersion curves was adopted by Suiker et al. [35] to determine critical speeds, while considering the ballast layer as an enhanced continuous medium to capture the influence of particle size of ballast. More recently, Connolly et al. [9] and Costa et al. [11] used dispersion curve analysis to calculate the critical speed of the track, where the track dispersion curve capturing rails, sleepers and ballast as rheological elements, was intersected with the natural ground dispersion curve as shown in Fig. 1b. The ground dispersion curves from the analytical model could be verified with the dispersion curves from field seismic tests such as Multichannel Analysis of Surface Waves (MASW)[31]. However, these analytical models were used to predict the displacements of rails and could not be extended to predict dynamic stresses in the major load-bearing track layers such as the ballast and capping layers.

Various numerical models have been used to address the dynamic amplification of track response using 2D and 3D Finite element methods (FEM) under moving loads[40,39,25,33,13,38]. To reduce the computational effort required for 3D modelling, 2.5D FEM or plane strain models were also developed by others (e.g., [10,5] to simplify the track conditions in the direction of train passage. These models were able to predict the stress distribution in the track in three dimensions and their variation with train speeds. It was also observed that the elasto-plastic and non-linear behaviour of the substructure materials and ground affected the critical speed of the track [6–8]. However, these models estimate critical speeds using numerous computations with different train speeds and extracting the train speed corresponding to the maximum response, thus requiring higher computational time for a detailed analysis.

It is important to note that the critical speeds calculated by both analytical and numerical methods are often high when compared to the common operating speeds in most countries including Australia. Several experimental and field investigations have shown that the condition of ballasted tracks degrades with time and the type of train loads and speeds[36,4,2,17,1,37,20]. For example, problems such as loss of ballast, ballast breakage, fouling and mud pumping are very frequent in Australian freight networks on the coastal areas[22,19]. From an operational point of view, it is pertinent to understand the dynamic response of the track at different stages during its lifetime through a critical speed analysis. In addition, the influence of axle loads on track degradation induced by dynamic track response needs to be quantified for accurate estimation of track performance, especially when the axle loads of freight trains increase beyond 25 T. It is also important to provide a more convenient pathway for practicing engineers to monitor the track substructure quality to analyse the real-time track response in relation to train speeds and axle loads. Moreover, most of the existing models for critical speed estimation have focussed on specific influential factors considered independently, such as the train speeds, the axle loads and the subgrade properties assumed to be constant with time. Also, these factors have not considered the effects of progressive subgrade degradation resulting from dynamic stress amplification. Also, most FE models require integration of new constitutive relationships which capture subgrade degradation (extent and rate). They are often limited to simulate the dynamic response under a single train passage and computationally challenging to simulate the changes in track dynamic response under large number of train passes (loading cycles).

In view of the above, the current study employs a combined methodology using analytical modelling and field investigation to provide greater insights on the influence of train speeds, axle loads and track condition on the dynamic track response. An analytical method is developed to estimate the critical speed of track, and to determine the effect of variations in track substructure conditions on its dynamic response. Rayleigh wave dispersion curves are drawn through a spectral analysis of the ground response to determine the critical speed, while quantifying the dynamic stress state. A geophysical survey of ballasted railway track conducted at a railway site in Chullora (near Sydney) is used to validate the analytical model. Using the analytical model, the influence of different problems observed in ballasted tracks on the stresses and critical speeds are analysed. Further, the analytical model is used to predict the critical number of axle load passes to induce unacceptable subgrade degradation that incorporates the combined influence of axle load, train speed and initial substructure characteristics on subgrade degradation.

Analytical method

A typical ballasted rail track is considered consisting of two parallel beams resting on concrete sleepers, considered herein as superstructure and an n-layered substructure with ballast as the topmost layer as shown in Fig. 2. In the model, the longitudinal, lateral, and vertical directions of the track are analyzed as x, y, and z, respectively. Positive (+) and negative (-) track movement and strains are considered in the downward and upward directions, respectively.

Superstructure dynamics

The track superstructure system is composed of rail, rail pads and sleepers. The steel rail is considered as a Euler-Bernoulli beam tied to

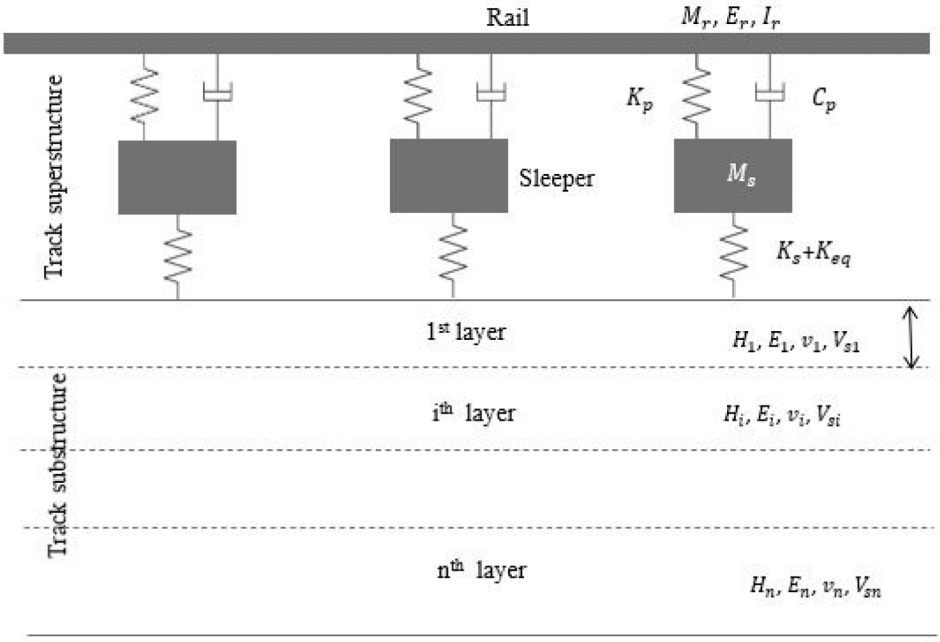

Fig. 2. Analytical model for ballasted railway track.

elastic (concrete) sleepers placed on the track substructure consisting of ballast, capping and other subgrade layers. A lumped mass spring-dashpot system is used to represent the track superstructure as shown in Fig. 2. Ks and Cs are the stiffness and damping coefficients of the rail pads, while M_s and K_s are the mass and stiffness of sleeper, and K_{eq} is the equivalent stiffness of the overall track substructure. Considering u_r and u_s as the vertical displacements of rail and sleeper, the motion equations for the superstructure system can be given as:

$$E_r I_r \frac{\partial^4 u_r}{\partial x^4} + M_r \frac{\partial^2 u_r}{\partial t^2} + C_p \frac{\partial u_r}{\partial t} + K_p(u_r - u_s) = P(t, V) \tag{1}$$

$$K_p(u_s - u_r) - M_s \frac{\partial^2 u_r}{\partial t^2} + K_{eq} u_s = 0 \tag{2}$$

In the wavenumber-frequency domain, Eqs. (1) and (2) can be written as:

$$\begin{bmatrix} EIk^4 + K_p - M_r\omega^2 & -K_p \\ -K_p & K_p - M_s\omega^2 + K_{eq} \end{bmatrix} \begin{Bmatrix} u_r(k,\omega) \\ u_s(k,\omega) \end{Bmatrix} = \begin{Bmatrix} P(k,\omega) \\ 0 \end{Bmatrix} \tag{3}$$

where, E_r and I_r are Young's **modulus and the second moment of inertia of the rail, M_s is the mass of the sleeper and rail together, K and C_d are the** stiffness and damping coefficient of the rail pad, respectively. The inclusion of a spring foundation (K_{eq}) has been incorporated to account for the stiffness contribution originating from the underlying substructure. In this study, K_{eq} was ignored since accurate calculations of the critical velocity could be achieved even without including it [29].

Substructure dynamics

The dynamic load transmitted by the superstructure generates R-waves in the ballast and other substructure layers. In a homogenous medium, the determination of propagation frequency of R-waves is relatively simple, but it becomes more complex in a layered media such as railway track due to the dispersion of R-waves generated at multiple frequencies. To determine the amplitude and frequency of R-waves generated in the track substructure, the P-wave and SV wave potentials in the substructure layers are combined using appropriate boundary conditions at the free top surface and subsequent layer interfaces[35].

In the current study, the authors have considered a n-layered track substructure with $n-1$ layers of thickness $h_{j..n-1}$ overlain on the n^{th} layer that is assumed as an elastic half-space. Considering the conservation of translation momentum in the longitudinal direction during R-wave propagation, the vertical σ^j_{zz}, shear σ^j_{xz} and longitudinal stresses σ^j_{xx}, in the j^{th} layer (for $j = 1$ to $n-1$) at a depth z_j can then be represented by:

$$\sigma^j_{zz} = e^{i(\omega t - kx)}\left\{b_{1j}A^j_{p1}e^{i\xi^j_{p1}Z} + b_{2j}A^j_{s1}e^{i\xi^j_{s1}Z} + b_{1j}A^j_{p2}e^{i\xi^j_{p2}Z} - b_{2j}A^j_{s2i}e^{i\xi^j_{s2}Z}\right\} \tag{4}$$

$$\sigma^j_{xx} = e^{i(\omega t - kx)}\left\{b_{3j}A^j_{p1}e^{i\xi^j_{p1}Z} - b_{2j}A^j_{s1}e^{i\xi^j_{s1}Z} + b_{3j}A^j_{p2}e^{i\xi^j_{p2}Z} + b_{2j}A^j_{s2}e^{i\xi^j_{s2}Z}\right\} \tag{5}$$

$$\sigma^j_{zx} = e^{i(\omega t - kx)}\left\{b_{4j}A^j_{p1}e^{i\xi^j_{p1}Z} + b_{5j}A^j_{s1}e^{i\xi^j_{s1}Z} - b_{4j}A^j_{p2}e^{i\xi^j_{p2}Z} + b_{5j}A^j_{s2}e^{-i\xi^j_{s2}Z}\right\} \tag{6}$$

Similarly, transient displacements in the longitudinal (u^j_x) and vertical (u^j_z) directions in the j^{th} layer can be written as:

$$u^j_x = -ie^{i(\omega t - kx)}\left\{kA^j_{p1}e^{i\xi^j_{p1}Z} + kA^j_{p2}e^{i\xi^j_{p2}Z} + \xi^j_{s1}A^j_{s1}e^{i\xi^j_{s1}Z} - \xi^j_{s2}A^j_{s2}e^{i\xi^j_{s2}Z}\right\} \tag{7}$$

$$u^j_z = ie^{i(\omega t - kx)}\left\{\xi^j_{p1}A^j_{p1}e^{i\xi^j_{p1}Z} - \xi^j_{p2}A^j_{p2}e^{i\xi^j_{p2}Z} - kA^j_{s1}e^{i\xi^j_{s1}Z} - kA^j_{s2}e^{i\xi^j_{s2}Z}\right\} \tag{8}$$

For the formulation of dynamic stresses and displacements in the half-space, the negative damping with increasing depth can be ignored, because the R-waves are generally restricted to the surface. Hence, the stress formulations for half-space can be simplified to:

$$\sigma^n_{zz} = e^{-i(\omega t - kx)}\left\{b_{1n}A^n_{p1}e^{i\xi^n_{p1}Z} + b_{2n}A^n_{s1}e^{i\xi^n_{s1}Z}\right\} \tag{9}$$

$$\sigma^n_{xx} = e^{-i(\omega t - kx)}\left\{b_{3n}A^n_{p1}e^{i\xi^n_{p1}Z} - b_{2n}A^n_{s1}e^{i\xi^n_{s1}Z}\right\} \tag{10}$$

$$\sigma^n_{zx} = e^{-i(\omega t - kx)}\left\{b_{4n}A^n_{p1}e^{i\xi^n_{p1}Z} + b_{5n}A^n_{s1}e^{i\xi^n_{s1}Z}\right\} \tag{11}$$

$$u^n_x = -ie^{-i(\omega t - kx)}\left\{kA^n_{p1}e^{i\xi^n_{p1}Z} + \xi^n_{s1}A^n_{s1}e^{i\xi^n_{s1}Z}\right\} \tag{12}$$

$$u^n_z = ie^{-i(\omega t - kx)}\left\{\xi^n_{p1}A^n_{p1}e^{i\xi^n_{p1}Z} - kA^n_{s1}e^{i\xi^n_{s1}Z}\right\} \tag{13}$$

Detailed derivation of the stresses and displacements is given in

Appendix-A. In Eqs. (5)–(9), A^j_{p1}, A^j_{p2} and A^j_{s1}, A^j_{s2} represent the amplitudes of P-wave and S-wave potentials in the ballast layer, respectively. In Eqs. (9) – (13), A^n_{p1} and A^n_{s1} represent the amplitudes of P-wave and S-wave potentials in the subgrade layer, respectively. The fundamental characteristics ω and k are the angular frequency and wavenumber of the R-waves generated in the substructure. The parameters $b_{1j}, b_{2j}, b_{3j}, b_{4j}, b_{5j}$ are functions of elastic modulus and poisons ratio of ballast and subgrade layers given in Appendix-A. The other parameters ξ^j_{p1},ξ^j_{p2} and ξ^j_{s1}, ξ^j_{s2} are the depth attenuation factors for P and SV waves given as:

$$\xi^j_{p,s,1,2} == \pm\sqrt{\frac{\omega^2}{C^{j\ 2}_{p,s}} - k^2} \tag{14}$$

where, C^j_p and C^j_s are the P-wave and S-wave velocities of the j^{th} layer, respectively. The equations (Eqs. (4)–(13) to calculate stress and displacements in the track layers contain unknown amplitude parameters, and they can be determined based on the boundary conditions applicable for R-wave propagation as explained below with the following assumptions:

a) At the surface of the ballast layer ($z = 0$), the vertical stress is equal to the dynamic stress imparted by the superstructure onto the sleeper-ballast interface, while the shear stresses can be neglected. The corresponding equations for calculating sleeper-ballast interface stresses are given in Appendix-B.
b) At other substructure layer interfaces, the stress and displacement compatibility conditions ($\sigma^i_{zz,xx,zx} = \sigma^{i+1}_{zz,xx,zx}$, $u^j_{x,z} = u^{j+1}_{x,z}$) are considered.

For a n-layer substructure, the boundary conditions give 4n-2 governing equations, which can be written as an eigen value problem: $CA = q$. The term C represents a 4n-2 x 4n-2 matrix with the elements of the matrix as a function of ω, k, geometry parameters and material parameters of the substructure layers. The vector A contains 4n-2 amplitude variables and q is the loading matrix. The dispersion curves of the track substructure can be derived by:

$$\det C(k, \omega, H, E) = 0 \tag{15}$$

Eq. (15) is a complex equation which was solved in this study using numerical solution where ω and k are iterated to check singularity of Eq. (15). Depending on the material properties of the substructure, Eq.15 gives multiple modes of R-waves[16], however in this study, only the fundamental mode is used for simplicity. This fundamental mode corresponds to the $\omega - k$ combination with lowest phase velocity as shown earlier in Fig. 1a. For predicting the dynamic track response, the dynamic stress imparted at the sleeper-ballast interface due to a single axle of a moving train has been considered, and the corresponding governing equations for dynamic stress calculation are given in Appendix-B.

Model validation

Ground dispersion curves

The proposed analytical model is first used to predict the dispersion cures of layered ground in relation to two previous studies[34,29]. Soil parameters are extracted from the respective studies as given in Table 1 and then used as input for the current analytical method; the corresponding dispersion curves are then plotted as shown in Figs. 3a and b. The dispersion curves are drawn in wave number-frequency domain for Sheng et al. [34] and phase velocity – frequency domain for Mezher et al. [29] to maintain consistency with the original studies as much as possible. The predicted dispersion curves show a clear agreement with that given by the respective studies at different modes of wave propagation in a layered ground. Different modes of wave propagation including the fundamental mode is predicted well by the proposed analytical model. Some minor discrepancies in model predictions are observed in Fig. 1b due to the iterative procedure considered herein to obtain different R-wave modes. This might be due to the precision of ω and k that is used to incorporate the dispersion curve data from Eq.15, which would have caused the model to overlook some of the intermediate peak values especially at low frequencies (~0–5 Hz). However, it can be observed from Fig. 3b that the model predicts different modes of

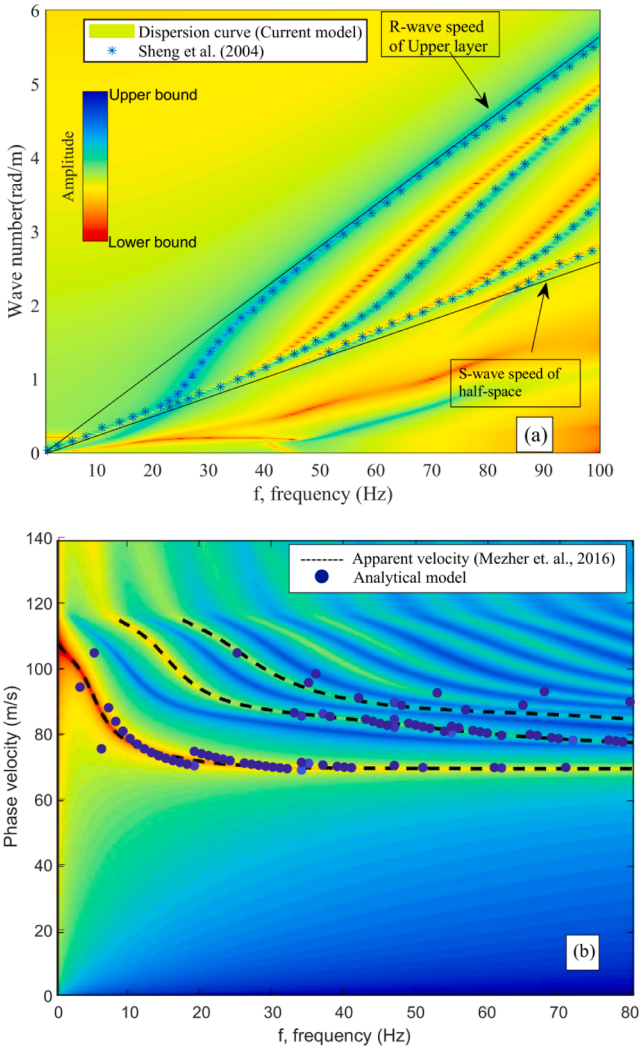

Fig. 3. Validation of subgrade dispersion curve with other methods from: (a) Sheng et al. [34] (b) Mezher et al. [29].

Table 1
Properties of track superstructure.

Rails			Railpads		Sleepers	
Elastic modulus, E_r (Pa)	Mass, M_r (kg/m)	Second moment of inertia,I	Stiffness, K_p (N/m)	Damping coefficient, C_p (N.s/m)	Mass, M_s per unit length of track (kg/m)	Stiffness, K_s (N/m)
$210e^9$	60	$30e^{-6}$	$5e^8$	$2.5e^5$	490	$60e^6$

dispersion curves with an acceptable accuracy.

Field study for ballasted track dispersion curve

To further demonstrate the capability of the model in predicting the dispersion curves of the ballast stratum as well as other substructure layers such as the capping, a field study was conducted in a site located in Western Sydney. The methodology involved MASW testing to determine the near-surface wave dispersion characteristics. In contrast to previous investigations[11,9], the survey was conducted on the top of ballast layer to benefit from the advantages as follows:

Repeat the survey on a ballasted track at different stages of track operations, in order to obtain a better understanding of the influence of track deterioration on the R-wave dispersion curves.
Estimate the improvement of the critical speed when different capping/sub-ballast layers and artificial inclusions are used in the track.

- Site conditions and test setup:

The substructure of the track was comprised of 300 mm thick ballast layer, a compacted capping layer of 150 mm in thickness and an underlying 50 mm thick drainage layer (Fig. 4). The lower sub-ballast layer was made of a 800 mm thick fill layer containing highly compacted bottom ash underlain by a subgrade composed predominantly of weathered shale and interspersed mudstone. MASW system used for this study consisted of a 24 channel Geode seismograph with 24 vertical geophones of 10 Hz capacity. The geophones were connected to the seismograph through split plate connectors and were placed on the top of ballast layer in the middle of the track and parallel to the rails as shown in Fig. 4. Considering the sleeper spacing at the test location, the geophones were placed at the midpoint between the sleepers with an equal spacing of 600 mm. Sufficient care was taken to maximise the contact between the geophone spike and the ballast assembly. The impact for surface wave generation is done using a 7 kg hammer and a square plate at a distance of 1.2 m. Based on previous investigations using MASW testing on ballast, the sampling frequency was set as 0.125 ms and recorded for a total duration of 0.25 s for the optimum signal.

- Site dispersion curve:

Different commercially available software was used to convert the seismic signal into dispersion curves. SeisImager 2D[15] was used for extracting the dispersion curve and for the inversion analysis. The phase velocity vs frequency distribution obtained at the site is plotted in Fig. 5, while the dispersion curve pertaining to the peak amplitude of seismic signal is also drawn for clarity. The shear wave velocities of substructure layers including ballast, capping and subgrade could be back calculated using the dispersion curve and the computed values are shown in Table 2. As expected, due to the presence of shale at a shallow depth (1–1.3 m) below the sleeper base, the corresponding elastic modulus was found to be relatively high (320 MPa) to be considered it as a stiff subgrade. The fill material at the site present between the capping layer and the moderately weathered shale showed a relatively smaller elastic

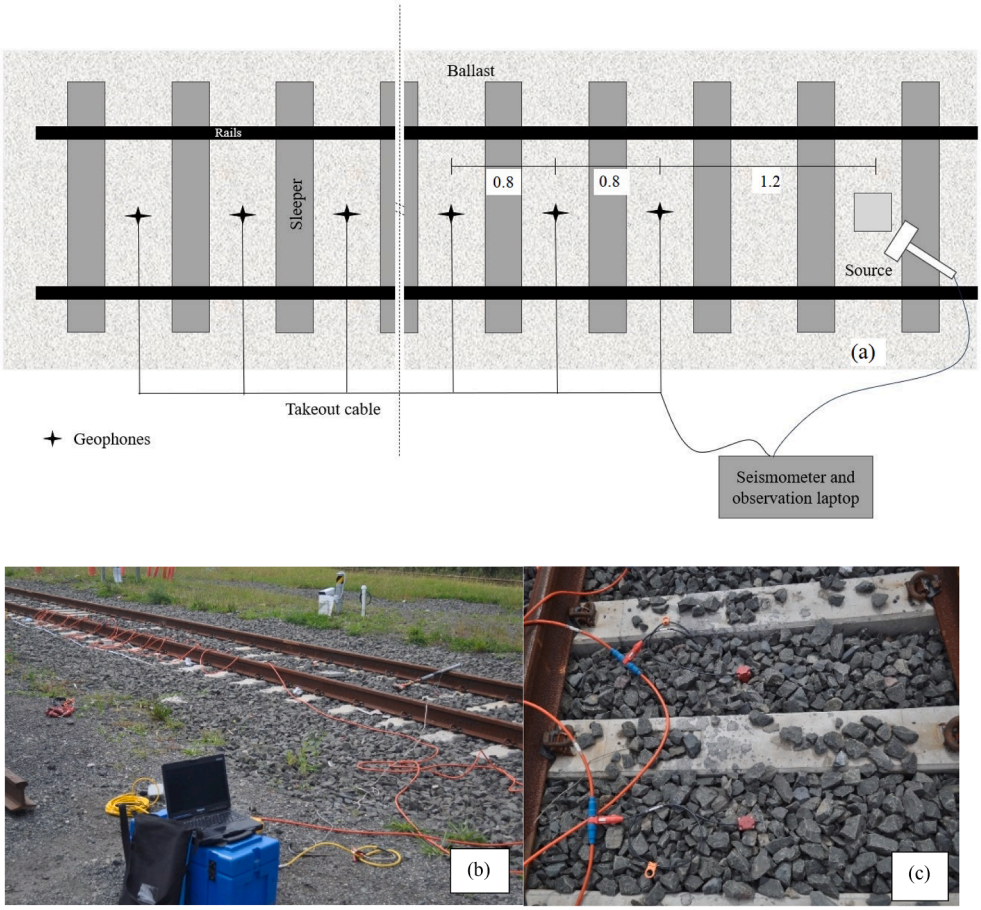

Fig. 4. (a)Schematic of MASW test setup (b)Field images of test setup (c)Placement of geophones on ballast surface.

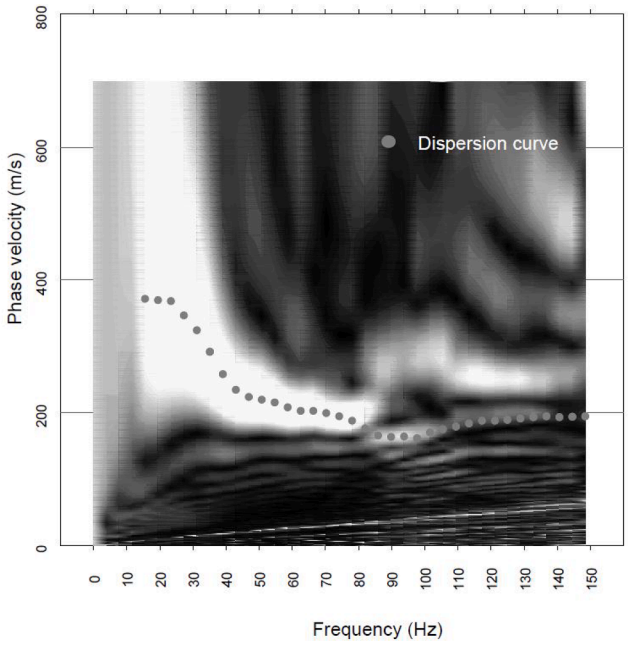

Fig. 5. Dispersion curve of ballasted track at Chullora, NSW.

Table 2
Material properties used for validation studies.

Validation: analytical and numerical models								
	Soft layer on stiff ground [34]				Soft ground [29]			
	E (MPa)	ν	ρ (kg/m^3)	H (m)	E (MPa)	ν	ρ (kg/m^3)	H (m)
Layer-1	60	0.44	1500	2	30	0.35	2000	2
Layer-2	360	0.49	2000	HS	40	0.35	2000	4
Layer-3	–	–	–	–	75	0.4	2000	HS
Field studies								
Ledsgard, Sweden [27]								
	E (MPa)	ν	ρ (kg/m^3)	H (m)	–	–	–	–
Crust	22.35	0.49	1500	1.1	–	–	–	–
Organic clay	6	0.49	1260	3	–	–	–	–
Clay-1	15.8	0.49	1475	4.5	–	–	–	–
Clay-2	31	0.49	1475	6	–	–	–	–
Clay-3	44	0.49	1475	HS	–	–	–	–
Field studies (Australia)								
	Chullora, NSW (Current field investigation)				Bulli, NSW, Australia [21]			
	E (MPa)	ν	ρ (kg/m^3)	H (m)	E (MPa)	ν	ρ (kg/m^3)	H (m)
Ballast	150	0.35	1660	0.3	150	0.35	1660	0.3
Capping	182	0.3	1800	0.2	180	0.3	1800	0.15
Fill	127.4	0.4	2000	0.5	–	–	–	–
Subgrade	320	0.24	2000	HS	50	0.4	2000	HS

*HS = halfspace.

modulus when compared to those of the ballast and capping layers. The elastic modulus of ballast back calculated in this study was slightly higher than the previously reported values of 100–120 MPa based on a model track in the laboratory[3]. The higher modulus observed at site can be attributed to the track being in operation for a few months, thus causing significant cyclic densification.

The layer properties in Table-2 were incorporated in the present analytical model to validate the field dispersion curve. A three-layer model was considered, where ballast and capping materials were considered together as a composite with an equivalent layer using the following equation:

$$E_{eq} = \frac{H_1 + H_2 + H_3 + ..}{\frac{H_1}{E_1} + \frac{H_2}{E_2} + \frac{H_3}{E_3} + ..} \tag{16}$$

Fig. 6 shows the dispersion curve predicted by the model compared with the dispersion curve extracted from MASW test. From the analytical predictions, two distinct modes of wave propagation can be identified and highlighted here as the 'fundamental mode' and the 'higher mode'. The fundamental mode matches quite well the dispersion curve obtained from the field. Further, dispersion curve for track superstructure (including the rail and sleeper assembly) plotted using Eq.3 is superimposed on to these curves. The intersection point shows a critical speed of 198 m/s (712 km/h), owing to the stiff shale subgrade.

Validation of transient displacements and stresses

In addition to the dispersion curves, the model was validated to predict the dynamic rail displacements at Ledsgard, Sweden when the train loading from X2000 train was simulated at different speeds. The layer properties considered for predictions are shown in Table 2. Fig. 7a shows the vertical displacements of the rail for an axle load of 12.5 tonnes at different speeds predicted by the analytical model, and the amplification of vertical displacements with increasing train speeds match very well with the field observations.

Similarly, the vertical stress distribution in the track substructure as predicted by the model was validated using the current field observations as well as with the data sourced from a past field study in Bulli, south of Sydney[21]. Fig. 7b shows the vertical stress distribution in the track substructure with depth from the sleeper base. The plotted stresses were measured and predicted below the rail seat. The predicted trend of vertical stresses matches well with the field observations. However, the proposed analytical model overpredicts the stresses at the ballast-capping interface in both studies, and this can be attributed to material damping of the ballast layer which was not considered.

Influence of different track problems on critical speeds

The longevity of ballasted railway tracks is highly dependent on the dynamic stresses experienced by the track layers under repeated train passages (i.e., cyclic loading). The granular substructure materials and underlying subgrade are prone to permanent deformations and degradation, the extent of which would depend on the magnitudes of stresses and the accompanying stress paths. Moreover, the freight railway lines

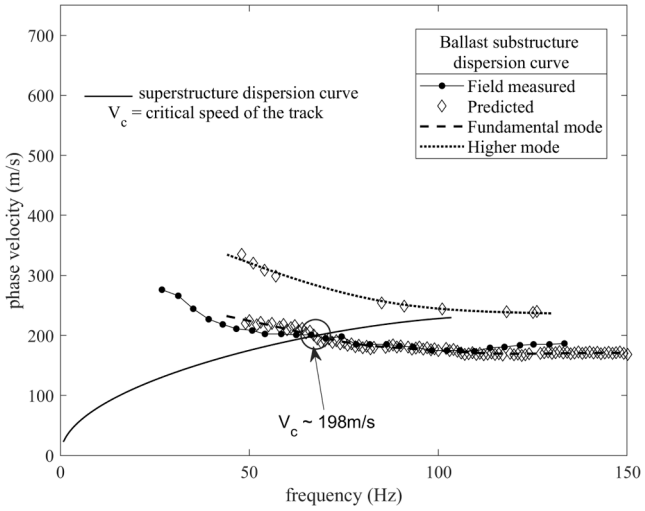

Fig. 6. Validation of dispersion curves with field measurements from Chullora.

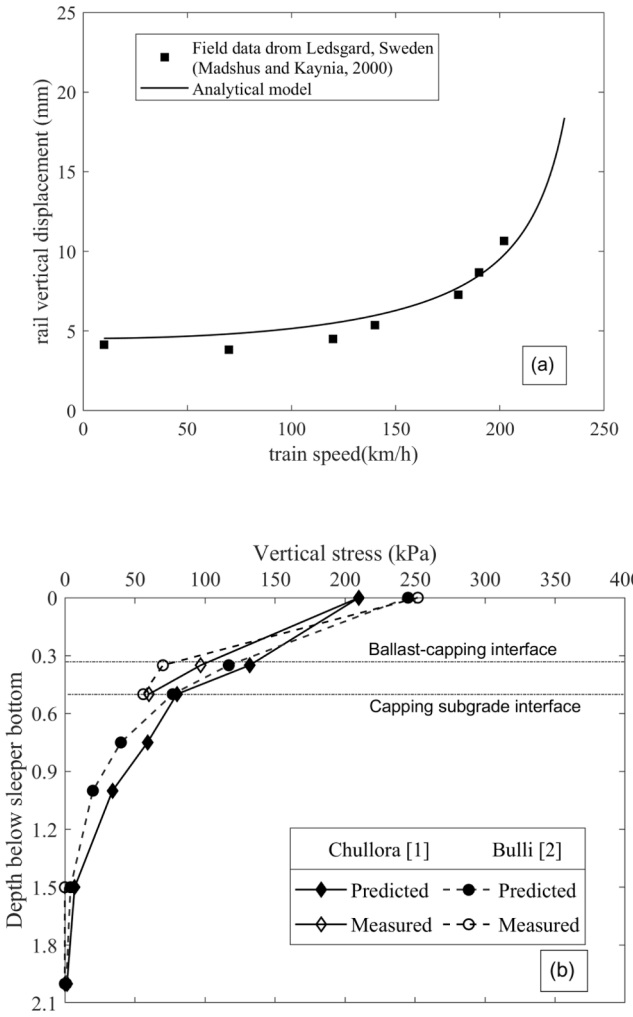

Fig. 7. Validation of dynamic response with field measurements: (a) rail vertical displacements (Ledsgard, Sweden), (b) vertical stress distribution at low train speeds for ballasted tracks in Australia.

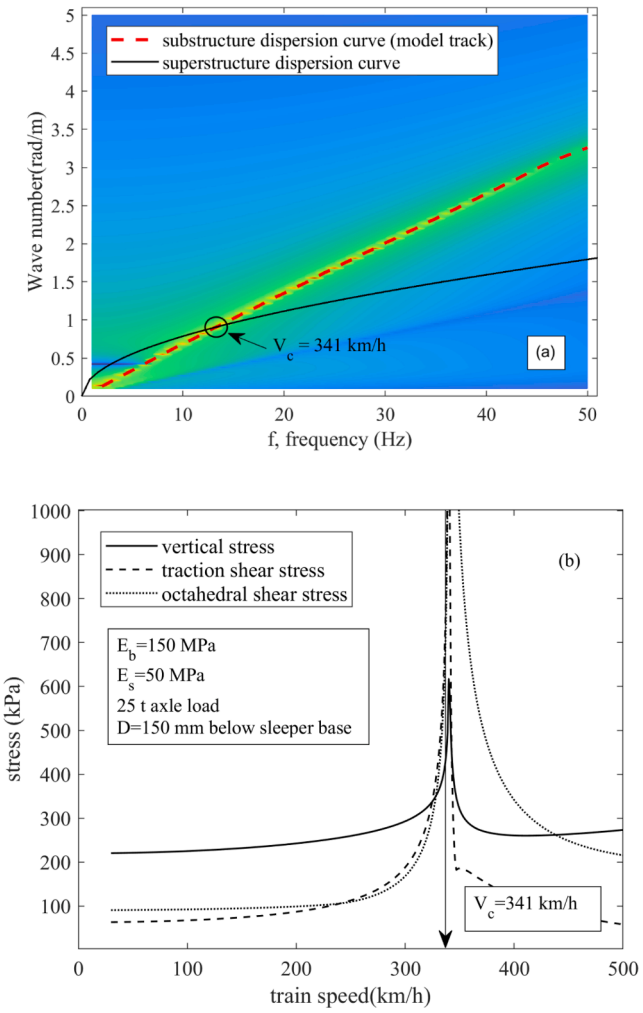

Fig. 8. Critical speed of ballasted railway track: (a) indirect vs (b) direct approaches (P = 25 T).

across the eastern coast of Australia with recently increased axle loads have reported that track problems such as mud pumping, breakage and fouling of ballast are common among the freight networks, leading to frequent maintenance. In this regard, it is important to understand the influence of common track problems on the dynamic response and critical speed of the track. In an operational point of view, accurate prediction of track degradation is crucial, because minimising the maintenance costs is of primary concern to asset owners.

Dynamic response in track substructure at different train speeds

The track substructure conditions from Bulli field study were considered for this purpose and the material properties are given in Table-2. The dispersion curves of both the track superstructure and substructure are shown in Fig. 8a, which indicates a critical speed (V_c) of 341 km/h when capping layer is not included. The variation of vertical, shear and octahedral stress at the midpoint of the ballast section (beneath the sleeper) with train speeds for a 25 t axle load train is plotted in Fig. 8b. The vertical stresses reach a maximum at a speed of about 341 km/h that matches perfectly with the critical speed estimated by the indirect approach. While the stress amplification is very gradual below 0.5 V_c, the stresses rapidly amplify as the train speeds approach V_c. It is also important to note that the tractional shear stress (in the direction of train passage) and the subsequent octahedral stresses also amplify close to critical speed.

Fig. 9a shows the variation of dynamic stresses with time as the train (axle load = 25 t) at different speeds. As the train speed is increased from 50 km/h to 180 km/h and then to 310 km/h, the vertical stresses as well as the shear stresses amplify. The resulting stress paths in the $\sigma_z - \tau_{xz}$ space follow a cardioid shape as shown in Fig. 9b, and the size of the stress path increases with the increasing train speed. Along with principal stress rotation, this amplification of stresses with train speeds affects the degradation of substructure layers and the resulting dynamic track response.

Effect of subgrade degradation on critical speeds

Indraratna et al. [23] reported that low plasticity clays found in the shallow coastal subgrade are prone to fluidization under impeded drainage under saturated conditions, especially following heavy rainfall or flooding. The shear modulus of fluidized subgrade soils reduces rapidly due to the build-up of excess pore water pressure triggered by the repeated passes of high axle loads. In the absence of sufficient drainage or for tracks which have no capping layer, fluidized subgrade can pump into the ballast layer causing significant fouling. Often, railway authorities restrict these adversely affected track sections to 20 % lower train speeds than usual operating speeds before the next maintenance cycle is scheduled. It is important to note that there are no existing technical guides explaining how the train speeds may affect subgrade degradation or how the reciprocal effects of degraded subgrade influence the track dynamics. The proposed analytical model is used to

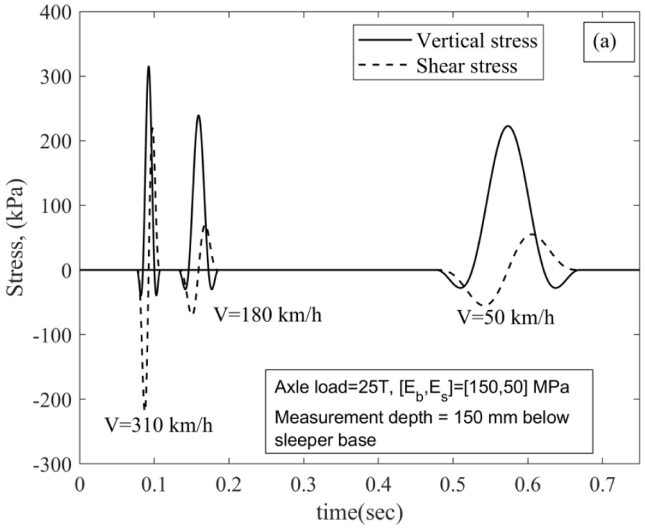

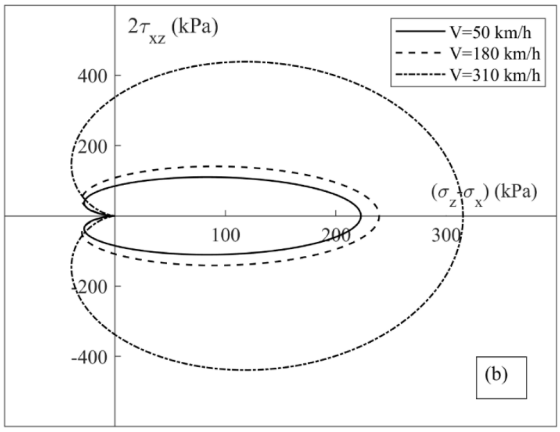

Fig. 9. (a)Dynamic stresses and (b)Stress paths in the track substructure layers at different train speeds.

simulate the subgrade degradation underneath the ballast layer and its effect on the critical speed. Subgrade degradation is considered using the degradation ratio (δ) as a function of the ratio of degraded shear modulus (G_d) to the initial shear modulus of the subgrade (G_s), as given below in Eq.17.

$$\delta = 1 - \frac{G_d}{G_s} \tag{17}$$

Fig. 10 shows the octahedral stress developed at shallow depth of subgrade, i.e., 100 mm below the ballast-subgrade interface with increasing train speed at different degradation ratios. Since mud pumping is a localised shallow phenomenon, the degraded subgrade is considered to have a limited thickness that is taken as 200 mm for the current analysis, as shown in Fig. 10. It is evident from Fig. 10 that the critical speed is affected significantly with the increase in degradation ratio, as it reduces from 341 km/h at$\delta_d = 0$ to 240 km/h at$\delta_d = 0.96$. Further, increased subgrade degradation causes quicker stress amplification, thus generating higher stresses at lower train speeds when compared to a subgrade with less degradation. However, at relatively low train speeds (V < 100 km/h), the stress experienced by the subgrade is smaller for a greater subgrade degradation. This means that more stress is now taken by the ballast layer that can reduce its longevity.

It is also observed that the rate of reduction in critical speed is non-linearly related to subgrade degradation as shown in Fig. 11a. When$(1-\delta_d) > 0.5$, the reduction of critical speed is not significant, while the critical speed decreases at a higher rate when$(1-\delta_d) < 0.5$.

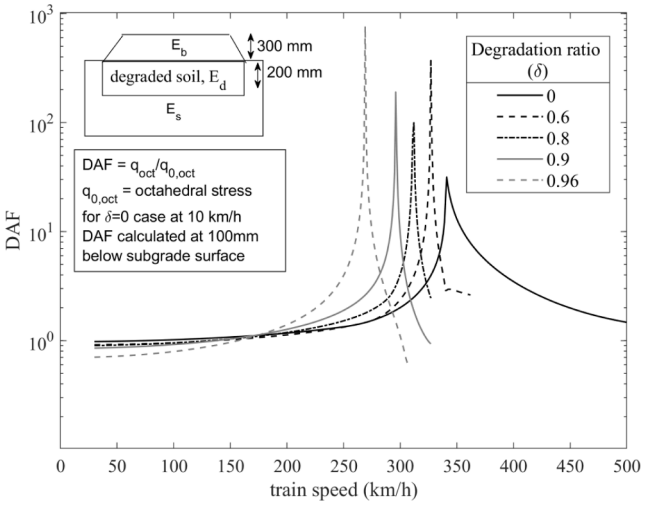

Fig. 10. Effect of subgrade degradation on dynamic amplification of stresses.

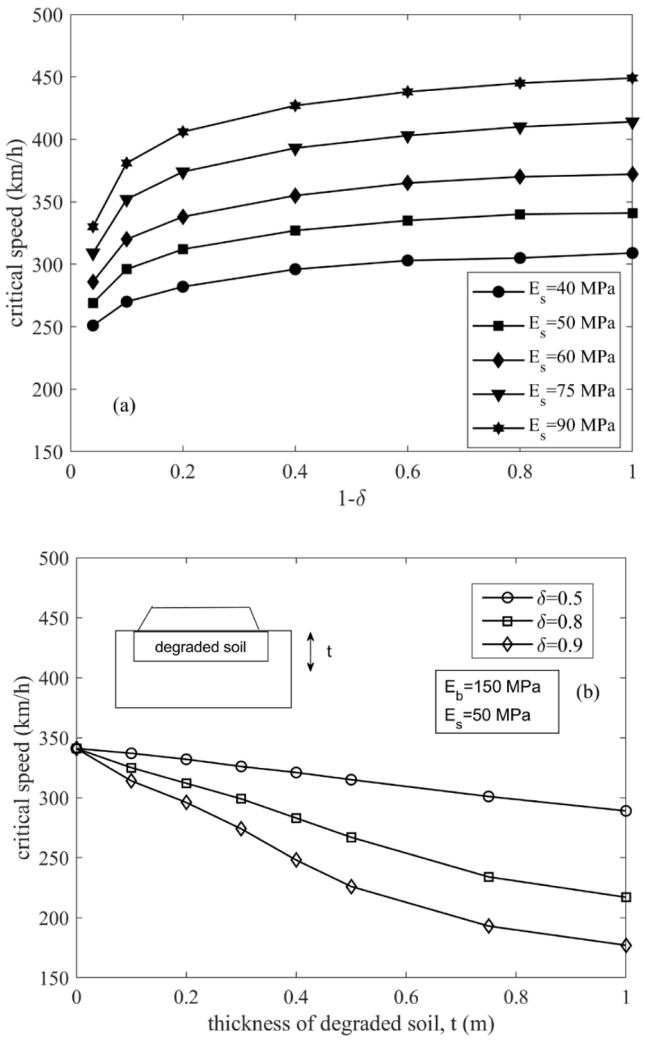

Fig. 11. Influence of mudholes on critical speeds for (a) different subgrade modulus (b) different mudhole thickness.

Further, the change in critical speed is influenced more when the initial subgrade modulus is higher, and this effect diminishes with a lower initial subgrade modulus. Fig. 11b shows the influence of the degraded

subgrade thickness on the change in critical speed. It can be observed that the thickness has little significance when the degradation ratio is moderate ($\delta_d = 0.5$); however, when the degradation ratio is relatively high ($\delta_d = 0.9$), increasing the subgrade thickness affects the critical speed more. When thickness of degraded soil is increased more than 0.5 m, the influence of thickness on critical speed gradually diminishes as the R-wave propagation depends completely on the degraded subgrade layer. This might be due to the characteristics of R-waves as they predominantly propagate in shallow depths and the properties of subgrade layer beyond certain depth becomes insignificant.

Ballast problems

The degradation of the ballast layer also affects the frequency of track maintenance. These problems include ballast loss (lateral movement) due to insufficient confining stress, ballast fouling due to particle breakage, and fouling caused by mud pumping or from coal falling from freight wagons. To understand the influence of ballast thickness on the critical speed, the analytical model can be used to predict the deviatoric stress at the ballast-subgrade interface as shown in Fig. 12a. The reduction in ballast thickness from 600 mm to 300 mm had resulted in the reduction of critical speed and premature amplification of stresses. Also, the stresses at the subgrade surface increase as the ballast thickness decreases, which leads to the subgrade becoming more susceptible to increased deformation. Also, the influence of ballast thickness on critical speed is found to vary with different subgrade conditions as shown in Fig. 12b. The reduction of critical speed with different ballast thickness is more pronounced for tracks having softer subgrade (i.e., lower subgrade modulus), while this effect diminishes for stiffer subgrades. When designing railways for high speeds, a greater importance should be given to problems such as ballast loss for track sections with softer subgrade rather than for tracks having stiffer subgrades.

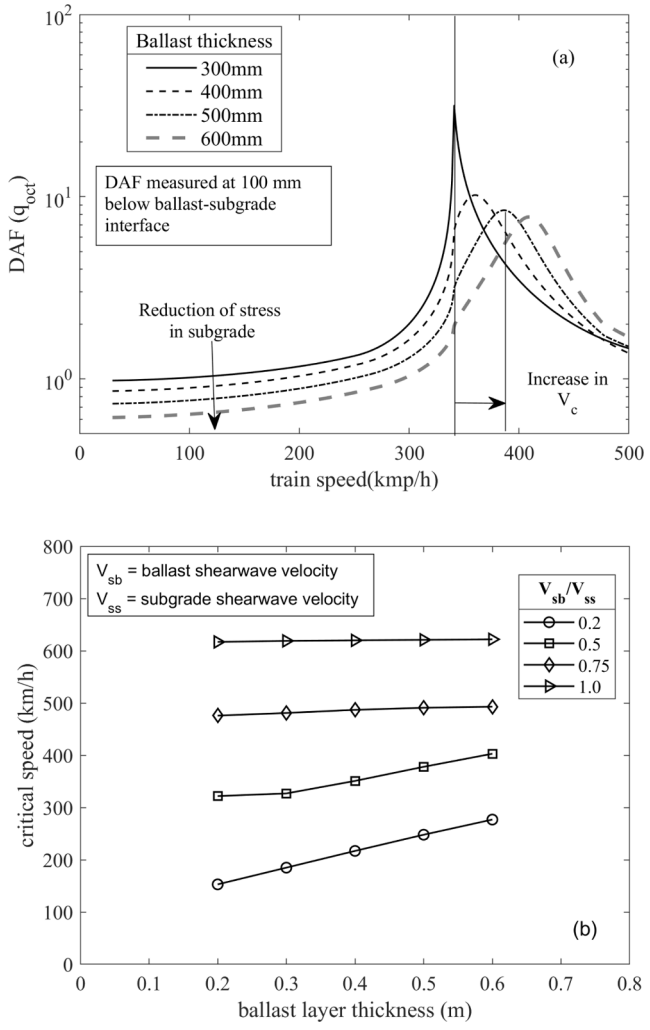

Fig. 12. Influence of ballast thickness on octahedral shear stresses and critical speeds.

Fig. 13 shows the influence of different extent of ballast fouling on the critical speed. Shear wave velocity data from Anbazhagan et al. [3] given in Table 3 is used herein to calculate the shear-wave characteristics of fouled ballast with clay, coal, and pulverised ballast for different fouling percentages. For the case of clay fouling, a 200 mm thick degraded subgrade modulus ($E_s = 10$ MPa) is considered as an important factor, because clay fouling mainly occurs due to pumping of the subgrade soil into the ballast layer. In contrast, for coal fouling the intact (no degradation) subgrade is considered, because coal fouling is caused by external conditions (e.g., vibration of overfilled carriages) which have no relation to the subgrade. In Fig. 13, dotted lines represent shear-wave velocities (V_s) of fouled ballast while the solid lines represent the critical speeds (V_c) of the track. The dotted lines indicate that coal fouling affects V_s more when compared to clay fouling. However, V_c decreases more with clay fouling, while coal fouling does not seem to affect the critical speed to any significant extent. Due to the degraded subgrade conditions in the cases of clay fouling, the overall R-wave propagation speeds is affected, hence the reason for the reduced critical speeds.

Influence of capping layer on critical speeds

In ballasted tracks, the capping layer is usually placed underneath the ballast layer to protect the deeper soft subgrade from excessive loading. The analytical model can be used to quantify the improvement in track dynamics including the critical speed when a capping layer is used. Fig. 14a shows the variation of octahedral stresses at a depth of 100 mm below the subgrade surface when a traditional capping layer with an elastic modulus of 180 MPa is used with a medium stiff subgrade of E = 50 MPa. As expected, the octahedral stress at the subgrade surface is reduced by the capping layer as shown in Fig. 14a. Also, an increase in critical speed is observed with the addition of capping layer and this improvement is higher when the thickness of capping is increased from 150 mm to 300 mm.

In recent times, a few studies [32,22,18] reported that blended mixtures of recycled mining waste (e.g., steel furnace slag, coal wash) and discarded rubber tyre derivatives (e.g., rubber crumbs) can be used as an alternative capping layer (Synthetic Energy Absorbing Layer,

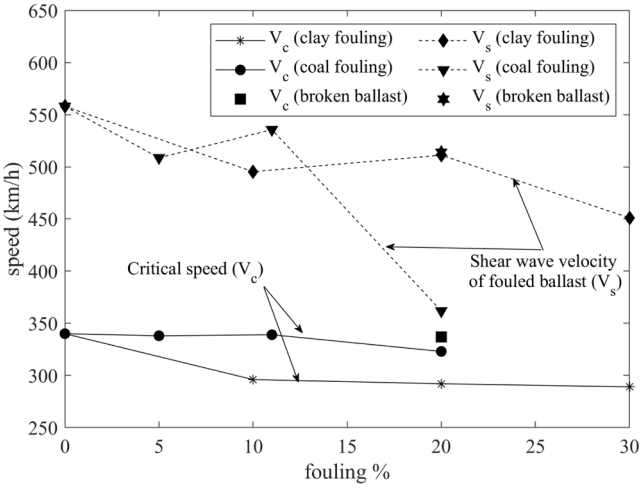

Fig. 13. Influence of ballast fouling on critical speeds.

Table 3
Material properties for ballast fouled with coal, clay and pulverised ballast (data from [3].

	shear wave velocity (MPa)	Poisson's ratio (υ)	density (kg/m^3)
Clean dense ballast	155	0.35	1636
Ballast + 11 %Coal	148.8	0.35	1807
Ballast + 20 %Coal	100.5	0.35	1770
Ballast + 30 %Clayey sand	125.3	0.35	1899
Ballast + 20 % clayey sand	142	0.35	2096
Ballast + 10 % clayey sand	137.6	0.35	1753
Ballast + 5 % coal	141.3	0.35	1675
Ballast + 20 % powdered ballast	142.75	0.35	2017

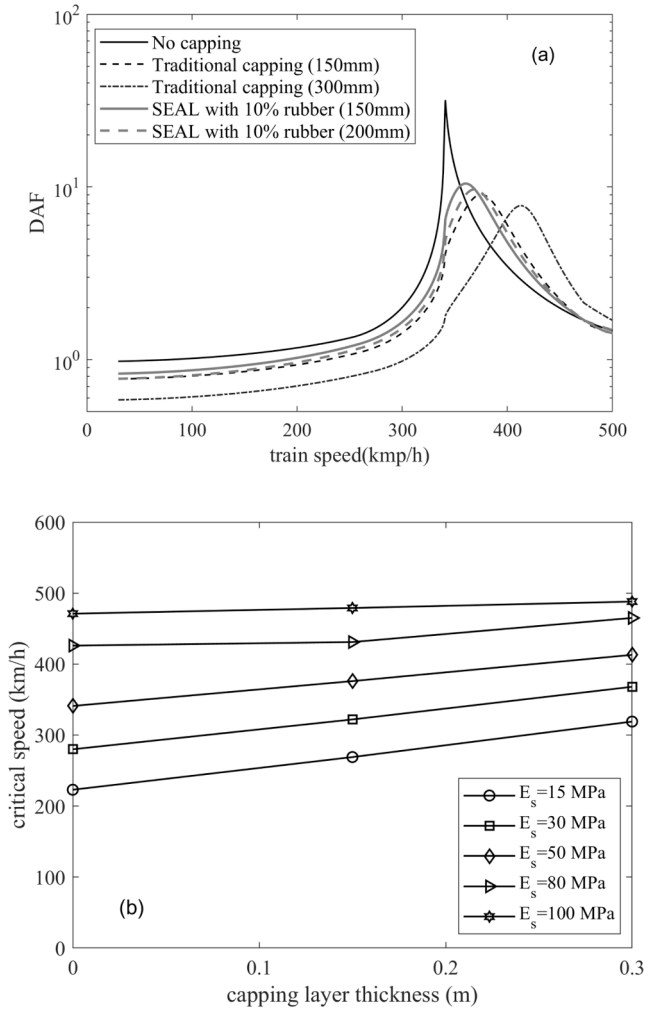

Fig. 14. (a)Improvement in track dynamic response with inclusion of capping layer (b)improvement in critical speed with capping for different subgrades.

SEAL), that also aids in increasing the energy absorbing capacity of track while reducing ballast breakage. As shown in Fig. 14a, using the SEAL material with an optimum rubber content of 10 % might not be as effective as a traditional capping layer (compacted sandy gravel) to increase the critical speeds of the track, and this is because of the lower elastic modulus (~90 MPa) of the blended waste mixtures. Since material damping (strain energy capacity) is not considered in the current analytical model, the advantage of the blended rubber material SEAL in reducing ballast breakage cannot be properly captured by this model. However, a 200 mm thickness of SEAL is found to perform similar to a 150 mm thick traditional capping layer. Further, for different subgrade conditions, the improvement in critical speeds is plotted in Fig. 14b. The capping layer is found to be more effective when it is used on softer subgrades, and that advantage diminishes as the subgrade becomes stiffer.

Influence of progressive subgrade degradation under repetitive loads

Previous sections established that the critical speed of a railway track is strongly governed by the substructure layer properties and their degradation characteristics. In most cases, dynamic stresses in the track substructure and the number of repeated loading cycles are the important driving factors for ballast/subgrade degradation. For example, trains with higher axle loads may cause greater stresses in the track layers leading to faster subgrade degradation. Hence, it is important to understand the combined influence of train speeds, axle loads and number of loading cycles on the resulting dynamic stresses generated and their effects on subgrade degradation during track operation. The empirical equation proposed by Nguyen et al. [30] represents the degradation of subgrade shear modulus prone to mud pumping (at shallow depth @ 1 m below sleeper base) with the number of loading cycles (N) and cyclic stress ratio (CSR), as given in Eq.18.

$$1-\delta = G_{sN}/G_{s1} = 1-\log(a.CSR)^b[\log N]^c \tag{18}$$

where, N represents number of loading cycles, G_{sN} is degraded subgrade modulus at Nth cycle, G_{s1} is the subgrade shear modulus during the first cycle. *a, b* and *c* are the empirical constants that affect the evolution of δ with N and are considered as 3.34, 0.69 and 2.5, respectively representing subgrade soil with a dry density of 1710 kg/m^3 [30]. CSR is considered as the ratio of octahedral stress to twice of lateral confining stress (CSR = $\frac{q_{oct}}{2\sigma_y}$). Eq.18 can be adopted in the current analytical model, and an iterative loop shown in Fig. 15 can be used to determine the influence of train speed and axle load under cyclic conditions (CSR) to estimate the value of critical N. The initial modulus of subgrade is considered as 50 MPa, which is typical of the natural clayey soil in the

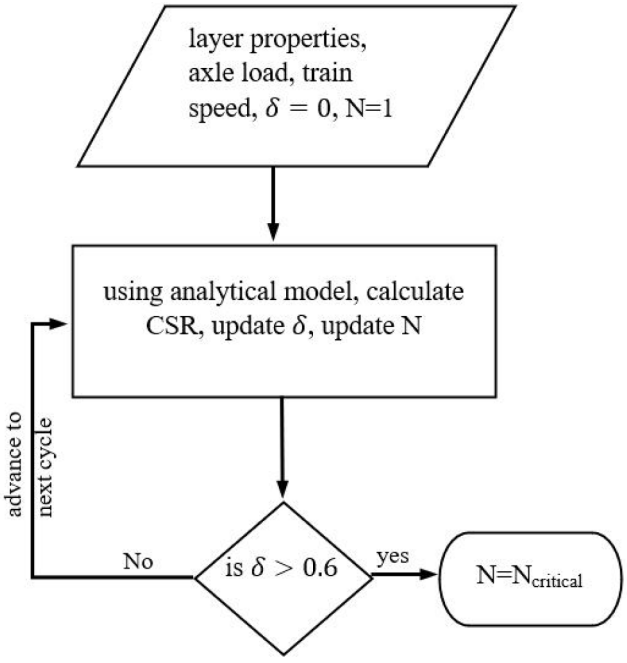

Fig. 15. Flow chart for determining critical number of loading cycles required for fluidization.

south-eastern coast of Australia (Indraratna et. al. 2010).

Fig. 16 show the number of cycles required for fluidization of the subgrade for three different axle loads (20 t, 30 t and 40 t) of freight trains running at different train speeds. Please note that the subgrade is considered as fully saturated with unfavourable drainage conditions. Also, δ>0.6 is considered as the threshold value in this study beyond which the degraded subgrade fluidizes[23]. It is observed from Fig. 16 that without a capping layer the subgrade reaches fluidization at approximately 711 cycles for 20 t axle train operating at 50 km/h. But for higher axle loads at 50 km/h, degradation occurs more rapidly within 100 cycles for 30 t and 42 cycles for 40 t. Also, $N_{critical}$ reduces with increasing train speeds from 50 to 180 km/h for all axle loads as the stresses in the subgrade layers amplify with train speeds.

For comparison, the number of loading cycles exerted on the subgrade under a typical iron ore train operated in Western Australia carrying 240 wagons (N_{train}) is plotted. The subgrade loading frequency of 5 HZ for a train running at 50 m/s speed is used as the benchmark for calculating N_{train} (Indraratna et. al. 2020). These trains which are very long do not allow the excess pore water pressure generated in the subgrade to dissipate until the whole train passes over the vulnerable location. It is to be noted that without a capping layer, for 20 t axle trains, $N_{critical}$ is found to be higher than N_{train} when the range of train speeds is below 120 km/h. However, for heavy freight trains with axle loads reaching 30 tonnes, the subgrade degrades within the duration of train passage even when travelling at low train speeds (50 km/h). This indicates that even though the subgrade was in a good condition before the train arrival, unfavourable drainage conditions can cause rapid degradation of the subgrade layer even during a single train passage. This effect becomes more severe under heavier axle loads of 40 t. When a 200 mm traditional capping layer is used, an improvement of $N_{critical}$ is observed for 20 t axle loads (e.g., 711 to 5748 cycles for 50 km/h), as shown in Fig. 16. However, this improvement gradually decreases as the axle loads increase from 20 t to 40 t. For very heavy axle loads (40 t), the findings from this study indicate that the subgrade degradation could not be controlled well by using a traditional capping layer that was sufficient to be used for lighter axle loads of 20 t.

Limitations

This analytical model provided a simple yet effective approach to capture the effect of track substructure conditions on dynamic track response. However, it is to be noted that the current analytical model at this point can only include vertical layering of the substructure and does not include any ground variations in the lateral or longitudinal directions. Furthermore, the model considers rail and sleepers to be free of defects or imperfections (e.g., rail corrugations) and the effect of any irregularities in these track elements on the dynamic response is ignored. The field investigation conducted in this study is limited to a single-track section, however, this will be extended to more sections of tracks with different subgrade properties in the future.

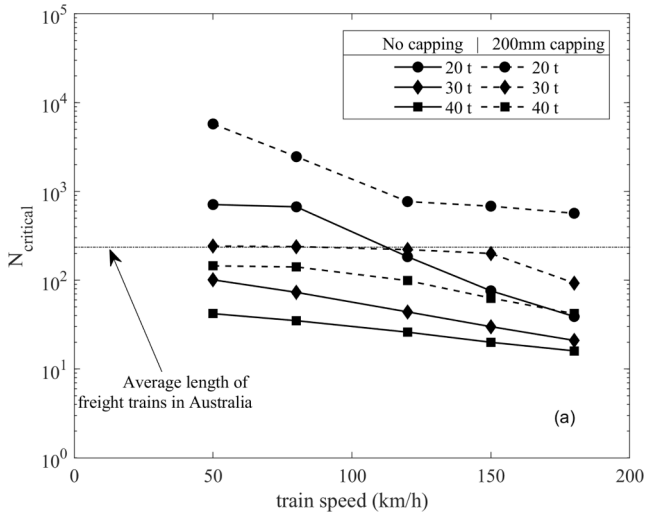

Fig. 16. Critical number of loading cycles required for fluidization of subgrade for different axle loads.

Conclusions

A rheological-continuum model was presented to analyse the influence of train speeds, axle loads and substructure conditions on the dynamic response of ballasted tracks under Australian track conditions. By considering a multi-layer continuum model for substructure layers including ballast, the model can be easily cross verified with MASW testing which can capture the current track conditions including ballast and subgrade degradation. After validation of the model with a field study and past numerical models, the observations from the model are as follows:

1. For ballasted tracks on softer subgrades, increasing the train speed caused an increase in the dynamic stresses in ballast and subgrade, including the vertical and traction shear stresses, resulting in principal stress rotation. The amplification in tractional shear stress was more than that of the vertical stress, leading to cardioid-shaped stress paths in the deviatoric stress space deviating from the conventional triaxial stress paths.
2. Occurrence of mud pumping represented by the proposed subgrade degradation ratio reduced the critical speed, while its influence was more pronounced when the thickness of degraded soil increased. For instance, consideringδ = 0.9 for railway track in Bulli, the critical speed reduced from 341 km/h to 296 km/h for subgrade (degraded) of 200 mm thickness, while it dropped further to 177 km/h when the thickness increased to 1 m.
3. For softer subgrade conditions ($\frac{V_{sb}}{V_{ss}}$ < 0.5), reduction of ballast thickness reduced the critical speed albeit by 20 %, however, this effect diminished when the ballast was underlain by a stiff subgrade ($\frac{V_{sb}}{V_{ss}}$ ~ 1.0).
4. Although ballast fouling due to coal adversely affected the critical speed (~5%), this effect was marginal when compared to the case of mud pumping (15 %-20 %).
5. In view of soil fluidization (following degradation) based on past laboratory studies on mud-pumping prone soils, a methodology was presented using the analytical model that could be used to calculate the critical number of loading cycles before the degrading subgrade could initiate mud pumping. When the tracks are used by very heavy freight trains (e.g., 40 tonnes axle load), a quicker fluidization was observed (i.e. $N_{critical}$ ⟨240) even while travelling at relatively low speeds (~50 km/h).
6. For mud-pumping tracks, the improvement in $N_{critical}$ with the addition of a capping layer becomes less prominent when axle loads are higher than 30 tonnes. Therefore, when these types of tracks are used by heavy freight trains, more extensive subgrade soil improvement may be necessary.

CRediT authorship contribution statement

Rakesh Sai Malisetty: Writing – review & editing, Methodology, Investigation, Formal analysis, Data curation, Conceptualization, Validation, Writing – original draft. **Buddhima Indraratna:** Writing – review & editing, Visualization, Validation, Supervision, Resources, Project administration, Methodology, Investigation, Funding acquisition, Formal analysis, Conceptualization.

Declaration of competing interest

The authors declare that they have no known competing financial interests or personal relationships that could have appeared to influence the work reported in this paper.

Data availability

Data will be made available on request.

Acknowledgements

The authors would like to acknowledge the financial support provided by Australian Research Council Linkage Project (200200915), Sydney Trains, Australian Rail Transport Corporation (ARTC), SMEC, Bentley Systems and Bestec instruments. The support from technical staff at the University of Technology Sydney (UTS) for carrying out field investigations is appreciated.

Appendix-A

For plane body wave motion in $x-z$ plane, the Cauchy stresses on an element can be given as:

$$\sigma_{xx} = \lambda(\varepsilon_{xx} + \varepsilon_{zz}) + 2\mu\varepsilon_{xx} \tag{A1}$$

$$\sigma_{xz} = \mu\varepsilon_{xz} \tag{A2}$$

$$\sigma_{zx} = 2\mu\varepsilon_{zx} \tag{A3}$$

$$\sigma_{zz} = \lambda(\varepsilon_{xx} + \varepsilon_{zz}) + 2\mu\varepsilon_{zz} \tag{A4}$$

Where, λ, μ are the Lames constants which can be expressed as

$$\lambda = \frac{E\nu}{(1+\nu)(1-2\nu)} \tag{A5}$$

$$\mu = \frac{E}{2(1+\nu)} \tag{A6}$$

And E, ν are the elastic modulus and Poisson's ratio of the layer. ε_{ij} is the first-order displacement gradient given as:

$$\varepsilon_{ij} = \frac{1}{2}\left(\frac{\partial u_i}{\partial j} + \frac{\partial u_j}{\partial i}\right) \tag{A7}$$

u_i and u_j are the displacements in the $i^{th} and j^{th}$ direction and can be represented as a function of compression wave potential and shear-wave potential as:

$$u_x = \frac{\partial \varnothing}{\partial x} - \frac{\partial \varphi_y}{\partial z} \tag{A8}$$

$$u_z = \frac{\partial \varnothing}{\partial z} + \frac{\partial \varphi_y}{\partial x} \tag{A9}$$

Φ^j and φ_y^j are the P-wave and SV wave potentials in the j^{th} layer can be given in $\omega-k$ domain as

$$\Phi^j = A_{p1}^j exp\left(-i\left(\omega t - kx - \xi_{p1}^j z\right)\right) + A_{p2}^j exp\left(-i\left(\omega t - kx - \xi_{p2}^j z\right)\right) \tag{A10}$$

$$\varphi_y^j = A_{s1}^j exp\left(-i\left(\omega t - kx - \xi_{s1}^j z\right)\right) + A_{s2}^j exp\left(-i\left(\omega t - kx - \xi_{s2}^j z\right)\right) \tag{A11}$$

Solving Eqs. A.1-A4 and A8, A.9 gives the stresses and displacements in the track substructure layers (Eq. (4)–(13), where the coefficients $b_{1j}, b_{2j}, b_{3j}, b_{4j}, b_{5j}$ are defined as a function of wave number k and Lame's constants as given below:

$$b_{1j} = -\lambda^j.k^2 - \left(\lambda^j + 2\mu^j\right)\xi_{p1}^{j\ 2} \tag{A12}$$

$$b_{2j} = 2\mu^j k\xi_{s1}^j \tag{A13}$$

$$b_{3j} = -\left(\lambda^j + 2\mu^j\right).k^2 - \lambda^j\xi_{p1}^{j\ 2} \tag{A14}$$

$$b_{4j} = 2\mu^j k\xi_{p1}^j \tag{A15}$$

$$b_{5j} = -\mu^j\left(k^2 - \xi_{s1}^{j\ 2}\right) \tag{A16}$$

Appendix B

Considering an axle with load q_0 moving on the rails at a constant speed V, the rail seat load q_r is calculated using the method proposed by ORE (1987) given as:

$$q_r = \frac{0.4q_d}{2} \tag{B1}$$

The dynamic load q_d imparted by the track superstructure to substructure at the sleeper-ballast interface is calculated by multiplying transmissibility ratio T_d to the incident load (q_0) on the rail. Transmissibility ratio is given as:

$$T_d = \frac{q_d}{q_0} = \frac{\sqrt{K_p^2 + \left(C_p\omega_l\right)^2}}{\sqrt{\left(K_p - (M_r + M_s)\omega_l^2\right)^2 + \left(C_p\omega_l\right)^2}} \tag{B2}$$

where, ω_l is the excitation frequency in the track superstructure caused by the moving axle and can be given as the ratio of train speed (in m/s) to the shortest spacing between axles $\omega_l = \frac{V\left(\frac{m}{s}\right)}{S_{axle}}$. The transmissibility ratio (T_d) varies from 1 to ∞, when the loading frequency, ω_l approaches the natural frequency of the superstructure. The influence of the axle on the rails extends to a distance of $-3\pi L/4$ to $3\pi L/4$ from the point of load application [12]. The variation of sleeper-ballast stress with time at x = 0 can be given by considering a cosine shape function with a wavelength λ=$3\pi L/2$

$$\sigma_{zd} = \frac{q_r \cos\frac{2\pi V}{\lambda}t}{A_e} \tag{B3}$$

where, A_e id the effective sleeper base area which is considered as one-third of the total base area.

References

[1] Abadi T, Pen LL, Zervos A, Powrie W. Improving the performance of railway tracks through ballast interventions. Proc Inst Mech Eng Part F: J Rail Rapid Transit 2018; 232:337–55.
[2] Anbazhagan P, Bharatha T, Amarajeevi G. Study of ballast fouling in railway track formations. Indian Geotech J 2012;42:87–99.
[3] Anbazhagan P, Indraratna B, Amarajeevi G. Characterization of clean and fouled rail track ballast subsurface using seismic surface survey method: model and field studies. J Test Eval 2011;39:831–41.
[4] Anderson WF, Fair P. Behavior of railroad ballast under monotonic and cyclic loading. J Geotech Geoenviron Eng 2008;134:316–27.
[5] Bian X, Cheng C, Jiang J, Chen R, Chen Y. Numerical analysis of soil vibrations due to trains moving at critical speed. Acta Geotech 2016;11:281–94.
[6] Castanheira-Pinto A, Colaço A, Ruiz JF, Costa PA, Godinho L. Simplified approach for ground reinforcement design to enhance critical speed. Soil Dyn Earthq Eng 2022;153:107078.
[7] Castanheira-Pinto A, Fernández-Ruiz J, Colaço A, Alves Costa P, Connolly DP. A simplified approach for predicting the non-linear critical speed of railway tracks. Transp Geotech 2022;37:100865.
[8] Connolly DP, Dong K, Alves Costa P, Soares P, Woodward PK. High speed railway ground dynamics: a multi-model analysis. Int J Rail Transp 2020;8:324–46.
[9] Connolly, D. P., Kouroussis, G., Woodward, P. K., Alves Costa, P., Verlinden, O. & FORDE, M. C. 2014. Field testing and analysis of high speed rail vibrations. *Soil Dynamics and Earthquake Engineering,* 67**,** 102-118.
[10] Costa PA, Colaço A, Calçada R, Cardoso AS. Critical speed of railway tracks. Detailed and simplified approaches. Transp Geotech 2015;2:30–46.
[11] Costa PA, Soares P, Colaço A, Lopes P, Connolly D. Railway critical speed assessment: A simple experimental-analytical approach. Soil Dyn Earthq Eng 2020; 134:106156.
[12] Esveld, C. 2001. *Modern Railway Track, 2nd Editon,* MRT-Productions, The Netherlands.
[13] Fernández-Ruiz J, Miranda M, Castro J, Medina Rodríguez L. Improvement of the critical speed in high-speed ballasted railway tracks with stone columns: A numerical study on critical length. Transp Geotech 2021;30:100628.
[14] Frýba, L. 1972. *Vibration of Solids and Structures under Moving Loads*. Thomas Telford.
[15] Geometrics 2009. SeisImager/SWTM manual windows software for analysis of surface waves. Geometrics San Jose, CA.
[16] Haskell, N.A. 1990. The Dispersion of Surface Waves on Multilayered Media. In Vincit Veritas: A Portrait of the Life and Work of Norman Abraham Haskell, 1905–1970, A. Ben-Menahem (Ed.). doi: 10.1029/SP030p0086.
[17] Hudson A, Watson G, Le Pen L, Powrie W. Remediation of mud pumping on a ballasted railway track. Procedia Eng 2016;143:1043–50.
[18] Indraratna B, Ngo T. Ballast railroad design: smart-uow approach. CRC Press; 2018.
[19] Indraratna B, Rujikiatkamjorn C, Salim W. Advanced rail geotechnology–ballasted track. CRC Press; 2023.
[20] Indraratna B, Ngo T, Ferreira FB, Rujikiatkamjorn C, Tucho A. Large-scale testing facility for heavy haul track. Transp Geotech 2021;28:100517.
[21] Indraratna B, Nimbalkar S, Christie D, Rujikiatkamjorn C, Vinod J. Field assessment of the performance of a ballasted rail track with and without geosynthetics. J Geotech Geoenviron Eng 2010;136:907–17.
[22] Indraratna B, Qi Y, Heitor A. Evaluating the properties of mixtures of steel furnace slag, coal wash, and rubber crumbs used as subballast. J Mater Civ Eng 2018;30(1): 04017251.
[23] Indraratna B, Singh M, Nguyen TT, Leroueil S, Abeywickrama A, Kelly R, et al. Laboratory study on subgrade fluidization under undrained cyclic triaxial loading. Can Geotech J 2020;57:1767–79.
[24] Kaynia AM, Madshus C, Zackrisson P. Ground vibration from high-speed trains: Prediction and countermeasure. J Geotech Geoenviron Eng 2000;126:531–7.
[25] Kouroussis G, Connolly DP, Verlinden O. Railway-induced ground vibrations – A review of vehicle effects. Int J Rail Transp 2014;2:69–110.
[26] Krylov VV, Dawson AR, Heelis ME, Collop AC. Rail movement and ground waves caused by high-speed trains approaching track-soil critical velocities. Proc Inst Mech Eng Part F: J Rail Rapid Transit 2000;214:107–16.
[27] Madshus C, Kaynia A. High-speed railway lines on soft ground: dynamic behaviour at critical train speed. J Sound Vib 2000;231:689–701.
[28] Madshus, C. & Kaynia, A. 2001. High-speed trains on soft ground: track–embankment–soil response and vibration generation. *Noise and vibration from high-speed trains.* Thomas Telford Publishing.
[29] Mezher SB, Connolly DP, Woodward PK, Laghrouche O, Pombo J, Costa PA. Railway critical velocity – Analytical prediction and analysis. Transp Geotech 2016;6:84–96.
[30] Nguyen TT, Indraratna B, Singh M. Dynamic parameters of subgrade soils prone to mud pumping considering the influence of kaolin content and the cyclic stress ratio. Transp Geotech 2021;29:100581.
[31] Park CB, Miller RD, Xia J. Multichannel analysis of surface waves. Geophysics 1999;64:800–8.
[32] Qi Y, Indraratna B. The effect of adding rubber crumbs on the cyclic permanent deformation of waste mixtures containing coal wash and steel furnace slag. Géotechnique 2022:1–10.
[33] Sayeed MA, Shahin MA. Three-dimensional numerical modelling of ballasted railway track foundations for high-speed trains with special reference to critical speed. Transp Geotech 2016;6:55–65.
[34] Sheng X, Jones C, Thompson D. A theoretical study on the influence of the track on train-induced ground vibration. J Sound Vib 2004;272:909–36.
[35] Suiker AS, Chang CS, De Borst R, Esveld C. Surface waves in a stratified half space with enhanced continuum properties. Part 1: Formulation of the boundary value problem. Eur J Mech-A/Solids 1999;18:749–68.
[36] Suiker AS, Selig ET, Frenkel R. Static and cyclic triaxial testing of ballast and subballast. J Geotech Geoenviron Eng 2005;131:771–82.
[37] Sun QD, Indraratna B, Nimbalkar S. Deformation and degradation mechanisms of railway ballast under high frequency cyclic loading. J Geotech Geoenviron Eng 2016;142:04015056.
[38] Tucho A, Indraratna B, Ngo T. Stress-deformation analysis of rail substructure under moving wheel load. Transp Geotech 2022;36:100805.
[39] Varandas JN, Paixão A, Fortunato E, Hölscher P. A numerical study on the stress changes in the ballast due to train passages. Procedia Eng 2016;143:1169–76.
[40] Yang L, Powrie W, Priest J. Dynamic stress analysis of a ballasted railway track bed during train passage. J Geotech Geoenviron Eng 2009;135:680–9.